See discussions, stats, and author profiles for this publication at: https://www.researchgate.net/publication/51809441

Electrochemistry at Nanoscale Electrodes: Individual Single-Walled Carbon Nanotubes (SWNTs) and SWNT-Templated Metal Nanowires

4 **AUTHORS**, INCLUDING:

Julie V Macpherson
The University of Warwick
175 PUBLICATIONS   **5,636** CITATIONS

Electrochemistry at Nanoscale Electrodes: Individual Single-Walled Carbon Nanotubes (SWNTs) and SWNT-Templated Metal Nanowires

Petr V. Dudin, Michael E. Snowden, Julie V. Macpherson,* and Patrick R. Unwin*

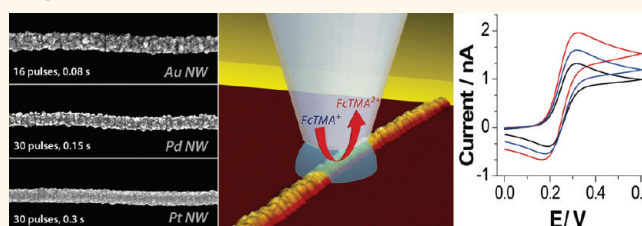Department of Chemistry, University of Warwick, Coventry, CV4 7AL, United Kingdom

I n the past two decades much effort has gone into the fabrication and application of nanoscale electrodes (NSEs), *i.e.*, electrodes with at least one dimension in the sub-100 nm regime, for both the quantification of fast electron transfer (ET) kinetics[1−6] and electroanalysis.[4,7]

The most popular NSEs are based on tapered or etched metal wires encapsulated by a variety of means to produce disk or conical electrodes.[2,8−12] While attractive in principle, the accuracy with which these NSEs can be used depends on microscopy characterization of the electrode geometry. This has often proved difficult due to the nanoscale dimensions of the electrodes, the presence of a large insulating coating, and the fact that they do not reside on a planar substrate. In these instances, NSE dimensions tend to be estimated from limiting current measurements, but this may not inform on the precise electrode geometry or dimensions. In the worst cases, kinetic data obtained on ill-defined NSEs may be miscalculated by an order of magnitude.[13,14]

A major, further drawback in the use of etching and sealing techniques for the fabrication of NSEs is the inherent variability in the electrode geometry and quality of the electrode-insulator seal, for electrodes produced using the same fabrication conditions. Thus, electrodes of this type are made by trial and error, and many procedures may be of low yield. The use of lithographic processing techniques to fabricate NSEs on planar substrates provides more control over electrode geometry, and NSEs are more amenable to high-resolution quantitative microscopic analysis;[15] however resist contamination is always a possible issue.

In this article we demonstrate a simple approach for the fabrication of nanowire (NW) electrodes (<100 nm in height), of a controllable dimension, based on metal-templated single-walled carbon nanotubes (SWNTs)[16,17] and pristine SWNT electrodes in their native form produced on an insulating support. Based on studies of related nanoband electrodes,[18,19] the NW structure is an interesting electrode geometry for electrochemical measurements due to the high intrinsic diffusion rates, associated with

ABSTRACT

Individual nanowires (NWs) and native single-walled carbon nanotubes (SWNTs) can be readily used as well-defined nanoscale electrodes (NSEs) for voltammetric analysis. Here, the simple photolithography-free fabrication of submillimeter long Au, Pt, and Pd NWs, with sub-100 nm heights, by templated electrodeposition onto ultralong flow-aligned SWNTs is demonstrated. Both individual Au NWs and SWNTs are employed as NSEs for electron-transfer (ET) kinetic quantification, using cyclic voltammetry (CV), in conjunction with a microcapillary-based electrochemical method. A small capillary with internal diameter in the range 30−70 μm, filled with solution containing a redox-active mediator (FcTMA$^+$ ((trimethylammonium)methylferrocene), Fe(CN)$_6$$^{4-}$, or hydrazine) is positioned above the NSE, so that the solution meniscus completes an electrochemical cell. A 3D finite-element model, faithfully reproducing the experimental geometry, is used to both analyze the experimental CVs and derive the rate of heterogeneous ET, using Butler−Volmer kinetics. For a 70 nm height Au NW, intrinsic rate constants, k^0, up to *ca.* 1 cm s^{-1} can be resolved. Using the same experimental configuration the electrochemistry of individual SWNTs can also be accessed. For FcTMA$^{+/2+}$ electrolysis the simulated ET kinetic parameters yield very fast ET kinetics ($k^0 > 2 \pm 1$ cm s^{-1}). Some deviation between the experimental voltammetry and the idealized model is noted, suggesting that double-layer effects may influence ET at the nanoscale.

KEYWORDS: nanowires · single-walled carbon nanotubes · electrochemistry · electrodeposition · kinetics · electron transfer · nanoscale electrodes

the small width (thickness) dimension, coupled with the high currents that flow (under potential control) as a result of the large length dimension.[18,19] NW dimensions can be accurately characterized using high-resolution microscopy and thus employed for *quantitative* voltammetric ET kinetic studies. While lithographically fabricated SWNT devices have been described,[20] photoresist contamination on the surface, causing partial blockage of the electrode, was identified as an issue.[21] The approach used herein avoids the need for photoresist or processing of electrodes,

ensuring electrode integrity, and allows for the production of multiple electrodes that can be addressed quickly and easily using the microcapillary electrochemical method (MCEM).[22]

RESULTS AND DISCUSSION

Fabrication of Metal NWs. Electrochemical synthesis of Pt, Pd, and Au NWs was performed in a three-electrode electrochemical cell with Pt-mesh serving as a counter electrode, Ag|AgCl (3 M KCl) as the reference electrode, and the SWNTs with a gold band contract as the working electrode (Figure 1). The SWNT-containing substrate was placed in the plating solution so that part of the gold band was also in contact with the electrolyte. The gold plating solution consisted of 0.1 mM $KAuCl_4$ in 0.2 M $NaClO_4$; Pd NWs were electrodeposited from 0.1 mM K_2PdCl_4 in 0.1 M $HClO_4$, and Pt NWs were electrodeposited from a solution containing 0.5 mM K_2PtCl_6 in 0.1 M $HClO_4$.

To gain insight into the current−voltage (CV) characteristics of metal deposition on SWNTs in different metal plating solutions, linear sweep voltammograms (LSVs) were recorded at 20 mV s^{-1} (Figure 2(a)) for the electrodeposition of Pt, Pd, and Au on SWNTs. For these studies randomly oriented two-dimensional SWNT networks[23,24] were used to amplify the electrochemical current, by assessing multiple nanotubes confined within the small area.[22,24−26] Solution-filled microcapillaries with an inner diameter of 80−85 μm, containing a counter/reference electrode, were employed to form the electrochemical cell for MCEM. As can be seen
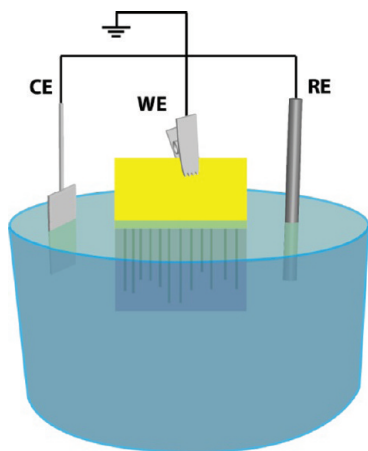

Figure 1. Schematic representation of the electrochemical setup for the templated electrodeposition of metal NWs onto ultralong SWNTs, where WE is the working electrode, CE is the counter electrode, and RE is the reference electrode.
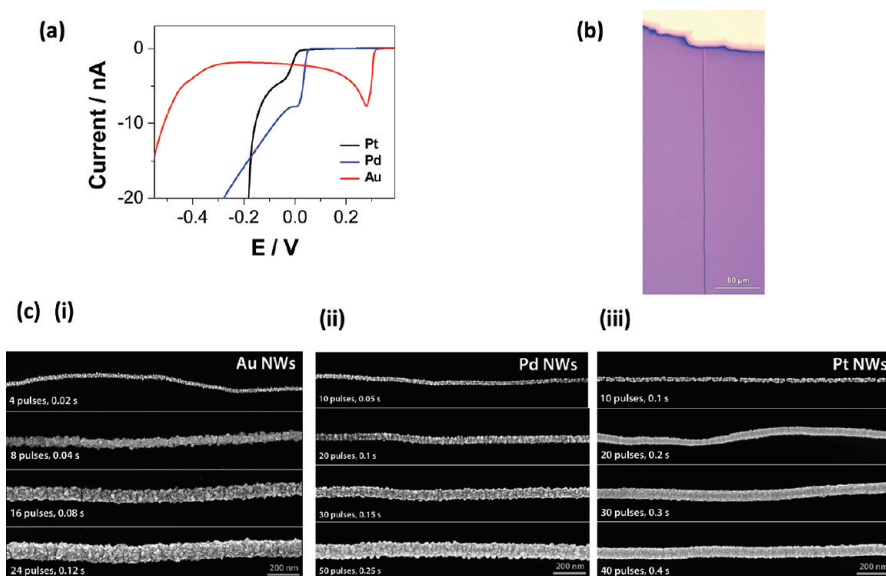

Figure 2. (a) LSVs for electrodeposition of Au (red), Pd (blue), and Pt (black) on a random network of pristine SWNTs using a microcapillary containing either 0.1 mM $KAuCl_4$ in 0.2 M $NaClO_4$, 0.1 mM K_2PdCl_4 in 0.1 M $HClO_4$, or 0.5 mM K_2PtCl_6 in 0.1 M $HClO_4$ at a scan rate of 20 mV s^{-1}. (b) Optical image of a Au NW electrodeposited on an isolated SWNT using 24 pulses of 5 ms duration at −0.45 V. (c) FE-SEM images of electrochemically deposited (i) Au NWs from a solution containing 0.1 mM $KAuCl_4$ in 0.2 M $NaClO_4$ using 5 ms deposition pulse at −0.45 V; (ii) Pd NWs from a solution containing 0.1 mM K_2PdCl_4 in 0.1 M $HClO_4$ using 5 ms deposition pulse at −0.25 V; (iii) Pt NWs from a solution containing 0.5 mM K_2PtCl_6 in 0.1 M $HClO_4$ using 10 ms deposition pulse at −0.25 V.
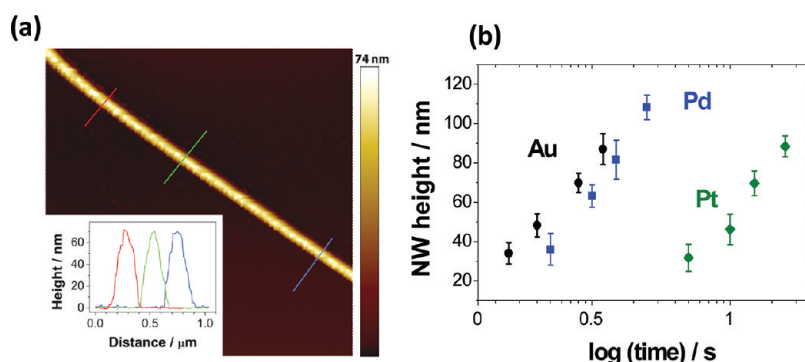
Figure 3. (a) AFM image (5 μm × 5 μm) of a Au NW deposited on a SWNT at −0.4 V using 16 pulses of 5 ms duration. (b) Plot of Pt, Pd, and Au NWs height (measured with AFM) against deposition time (number of pulses, hence integral time). The error bars correspond to 1 standard deviation from the mean value.

in Figure 2(a), electrodeposition of Au starts much earlier (*ca*. +0.35 V *versus* Ag/AgCl) than Pt and Pd (*ca*. 0 V). However, for the case of oxygen reduction, Au is significantly less electrocatalytic than Pt or Pd, as evidenced by the onset of oxygen reduction at potentials more negative than −0.4 V.

To deposit metal NWs, a potential pulse technique was used, with the aim of maximizing the surface coverage of nuclei on the SWNT sidewall, by both applying a high driving electrodeposition potential and keeping the pulse duration short to confine nuclei diffusion fields.[25] Between each pulse the system was returned to open circuit and a wait time of 10 s employed. In this study, the optimal potential/time conditions for the three metals were −0.45 V using 5 ms pulses (Au NWs, Figure 2(b i)), −0.25 V using 5 ms pulses (Pd NWs, Figure 2(b ii)), and −0.25 V using 10 ms pulses (Pt NWs, Figure 2(b iii)). A longer pulse time and higher salt concentration (0.5 mM) was employed for Pt, as Pt nucleation on SWNTs is known to be kinetically slower,[22] compared to Pd[22] and Au.[25]

The number of potential pulses employed directly influenced the size of the resulting NWs, as illustrated by the field-emission scanning electron microscopy (FE-SEM) images shown in Figure 2(c). FE-SEM revealed the deposited NWs to be contiguous and polycrystalline in nature. It is important to note that the use of a photoresist-free protocol is essential for the electrodeposition of contiguous NWs. For comparison with the approach herein, we created SWNTs that had been processed with photoresist, similar to previously demonstrated SWNT devices,[20] which was then removed as effectively as possibly. Photoresist contamination was found to impact significantly on the nucleation density, resulting in a reduced number of nuclei when using the same electrodeposition procedures, as shown in Supporting Information 1 (SI-1). This is not surprising, as photoresist contamination of SWNTs impedes or blocks electron transfer.[20,21]

Both optical microscopy (Figure 2(b)) and FE-SEM (Figure 2(c)) revealed the Pd and Au NWs (produced as described) to be continuous for ~1 mm in length. In contrast, the Pt NWs were continuous for only ~300−400 μm, most likely resulting from the slower nucleation kinetics. At longer distances, distinct metal nanoparticles (NPs) were observed. This behavior can be attributed to ohmic drop along the length of the SWNT,[16,27] which results in a reduced driving force for electrodeposition at further distances from the Au band contact.

A representative AFM image of an Au NW of height ca. 70 nm, fabricated using a 16 potential pulse program, is shown in Figure 3(a). For Au, the smallest contiguous NW that could be produced was 34 ± 5 nm (in height), which is smaller than previously reported electrochemical methods for metal NW formation.[17,28] For Pd and Pt the smallest NWs (in height) were 36 ± 7 and 32 ± 5 nm, respectively. Figure 3(b) shows the dependence of average NW height (measured with AFM) on the integral deposition time, *t*, which equates to the *number of pulses × pulse duration* for all three metals. It is evident that the NW height can be controlled with good precision *via* the number of pulses applied.

Voltammetry at NWs. Among the three electrodeposited metal NWs, Au generally exhibits the widest potential window in aqueous solutions and shows less voltammetric features for surface processes over a wide potential range.[29] Polycrystalline Au NWs were thus selected for further electrochemical studies of redox reactions of dissolved species, using the MCEM setup.[16,25] Using MCEM, the solution (confined by the microcapillary) is positioned over an area of the NW of interest (connected as a working electrode) and an electrochemical measurement is made. This approach has several advantages: (i) the area of interest does not need to be electrochemically isolated from solution using photoresist materials, ensuring that NW (and SWNT) surfaces can be studied in pristine form; (ii) many measurements can be made quickly on the same sample, containing many NWs or SWNTs, by simply moving the capillary to a new location.

Even though of nanoscale dimensions, Au NWs were clearly visible using an optical microscope
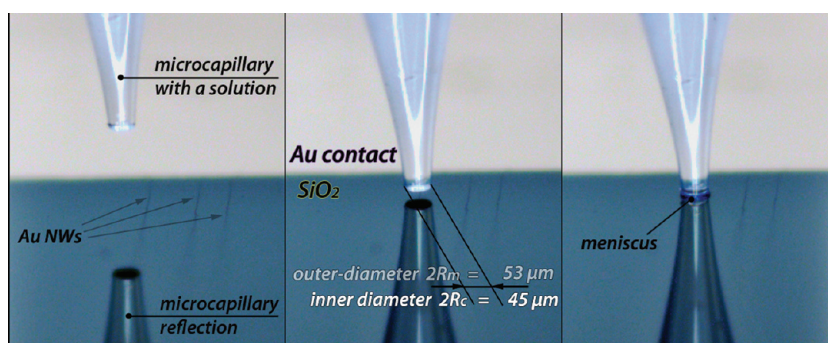
Figure 4. Series of snapshots from the video camera showing the process of microcapillary positioning over a Au NW and contact of the solution meniscus with the NW electrode.
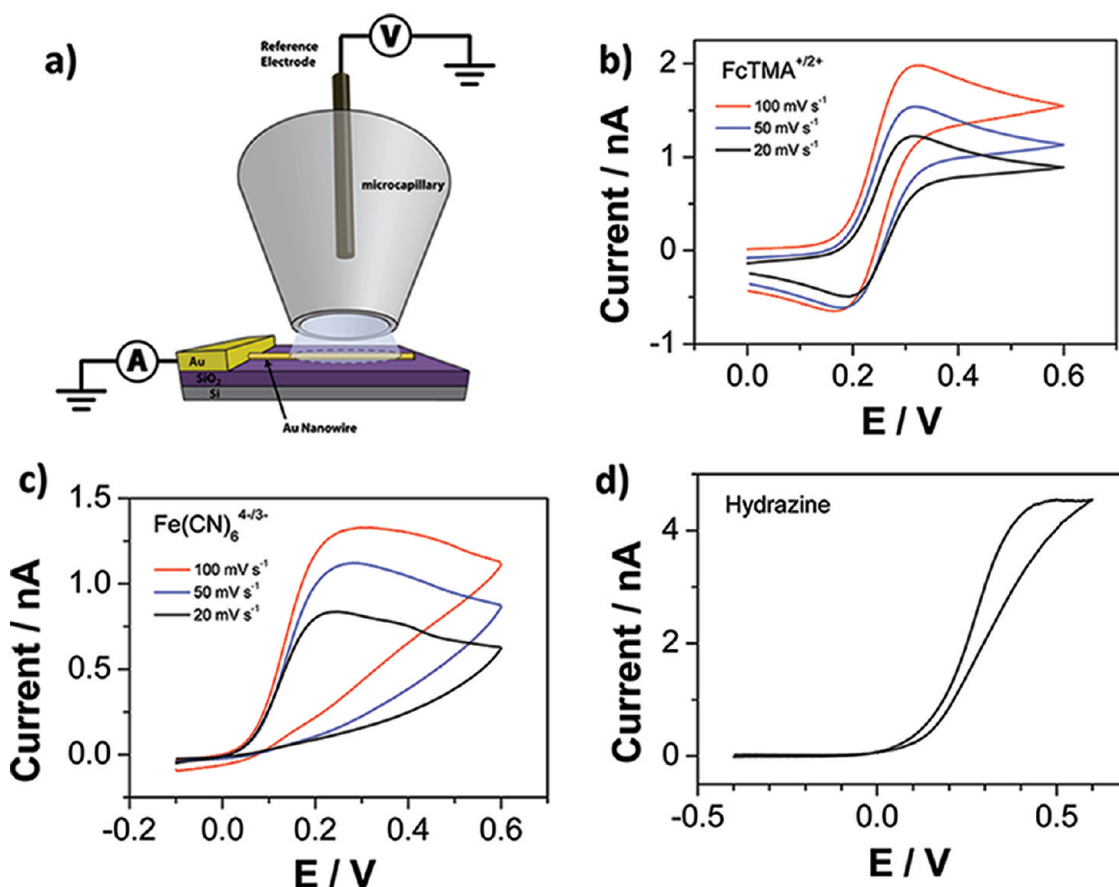

Figure 5. (a) Schematic of the microcapillary experiment involving positioning a microcapillary cell, containing the solution of interest, over a metal NW (optically visible) lying on an insulating SiO_2 substrate and electrically connected to an evaporated gold contact. (b) CVs for 1 mM $FcTMA^{+/2+}$ oxidation in 0.2 M $NaClO_4$ over a 70 nm Au NW; (c) CVs for 1 mM $Fe(CN)_6^{4-/3-}$ oxidation over a 70 nm Au NW; (d) CV for oxidation of 1 mM hydrazine in 0.1 M phosphate buffer solution (pH 7.2) at a 70 nm Au NW.

(due to a diffraction effect), and the microcapillary could thus be easily and quickly positioned over the NW, aided by a camera (Figure 4). A schematic of the experimental arrangement is shown in Figure 5(a). Prior to the experiment, the microcapillary was filled with the solution of interest, and a freshly chlorinated Ag wire served as a counter/reference electrode.[25] All further electrode potentials in MCEM measurements are quoted with respect to the chlorinated silver wire.

The contact (meniscus) radius (R_m) of the microcapillary was evaluated accurately by optical or electron microscopy from a salt residue footprint after voltammetric measurement, which has been shown to be an accurate method.[22] In general, R_m was slightly larger than the microcapillary radius (R_c), which was also determined accurately by optical microscopy. The glass of the microcapillary never contacts the surface, thus avoiding any damage to the Au NWs.
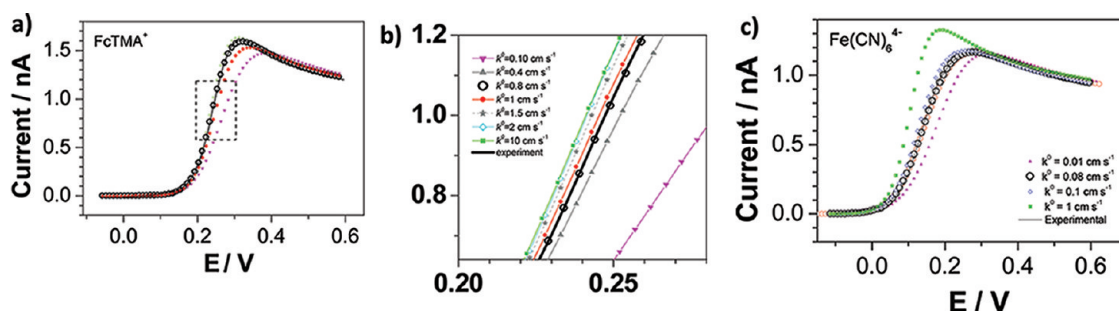
Figure 6. (a) Experimental voltammogram (black line) for the oxidation of 1 mM FcTMA$^+$ in 0.2 M NaClO$_4$. (b) Magnified dashed area in (a) of the simulated voltammetric response for FcTMA$^+$ oxidation for k^0 in the range 0.1–10 cm s^{-1} ($\alpha = 0.5$) compared to experiment. (c) Experimental response (black line) for oxidation of 1 mM Fe(CN)$_6^{4-}$ over a 70 nm Au NW at 50 mV s^{-1} and simulations (dotted) based on Butler–Volmer ET for k^0 in the range 0.01–1 cm s^{-1} and $\alpha = 0.5$.

Furthermore, the ability to measure these electrochemical cell parameters, in addition to the NW size, with high precision allowed the construction of faithful models for the electrochemical response, with few adjustable parameters.

Figure 5(b) shows typical CVs recorded at scan rates of 20, 50, and 100 mV s^{-1} for the one-electron oxidation of (trimethylammonium)methylferrocene cation (FcTMA$^+$, 1 mM in 0.2 M NaClO$_4$) at a 70 nm Au NW using the MCEM setup with $R_c = 25\,\mu m$ and $R_m = 32\,\mu m$. The observed CVs are slightly peak-shaped as a result of a contribution of linear diffusion during the time period of a CV. Figure 5(c) shows typical CVs for the one-electron oxidation of 1 mM Fe(CN)$_6^{4-}$ (in 0.1 M NaClO$_4$) recorded at scan rates of 20, 50, and 100 mV s^{-1} using a micropipet with $R_c = 22.5\,\mu m$ and $R_m = 28\,\mu m$. The forward portion of the Fe(CN)$_6^{4-/3-}$ CV is more drawn out than for FcTMA$^{+/2+}$, indicating a slower rate of ET,[30,31] and the current on the back scan shows significant hysteresis. The latter is likely to be a consequence of the adsorption of products and/or the formation of Prussian blue[31,32] during the course of the experimental measurement. Although Fe(CN)$_6^{4-/3-}$ is used for investigating many electrode geometries, it is known to be a rather complex couple showing nonideal redox behavior,[30,33] and such effects become very noticeable in these measurements due to the very high fluxes to the NW electrodes.

Figure 5(d) shows a characteristic CV for the electro-oxidation of 1 mM hydrazine (HZ) in 0.1 M phosphate buffer (pH 7.2) solution at a 70 nm Au NW electrode, at 100 mV s^{-1}, using a microcapillary with $R_c = 21\,\mu m$ and $R_m = 24\,\mu m$. This is known to be an inner-sphere redox process,[34] such that on a bare SWNT oxidation of HZ does not take place,[29] but is catalytically promoted through the use of various metal electrodes, including Au.[35] Interestingly, the CV shows a clear steady-state oxidation current, as a consequence of the irreversible nature of the ET reaction coupled with the effect of the diffusion profile in the tapered capillary (Figure 5(a)). Here, the $E_{1/2}$ value is ca. 190 mV more positive than values reported for Au NP-functionalized SWNT

network electrodes. Moreover, the calculated value of 145 mV for the diffusion-corrected Tafel slope for HZ oxidation on the Au NW is ∼55 mV greater than for both polycrystalline Au[35,36] and Au NP-functionalized SWNTs.[29] These differences indicate significant kinetic effects for HZ electro-oxidation at the Au NW electrode as a consequence of the dramatically increased fluxes to the NW electrode.

A 3D finite-element model was developed to simulate the CV current–voltage response for quasi-reversible ET kinetics at a cylindrical tube in the MCEM setup under conditions of diffusion-only mass transport. Briefly, the time-dependent diffusion of the reactant was solved within an approximation of the MCEM geometry with a cylinder representing the NW or SWNT. Two planes of symmetry were used to enhance the simulation efficiency. Simulations were employed to extract the heterogeneous electron transfer rate constant, k^0, from the forward scan of the recorded CVs. We assume a symmetrical reaction pathway; hence $\alpha = 0.5$ (SI-2).

The important geometric features are R_m, R_c, the capillary cone semiangle ($\theta = 10 \pm 2°$, as measured with optical microscopy), and the NW height (representing the NW as a cylinder, lying on an inert substrate). The height, h, of the meniscus in contact with the surface was estimated from *in situ* optical images (e.g., Figure 4) using the camera and was typically 15 μm. Given that R_m is only slightly larger than R_c, it was reasonable to approximate the shape of the meniscus as a straight boundary in all the simulations. Butler–Volmer kinetics were solved at the NW/SWNT surface to determine k^0. A more detailed description of the COMSOL modeling can be found in SI-2.

Figure 6(a) shows a LSV for 1.0 mM FcTMA$^+$ oxidation (in 0.2 M NaClO$_4$) recorded at 50 mV s^{-1} (solid black line), using a Au NW electrode of height 70 nm and length 64 μm ($R_m = 32\,\mu m$) and simulated LSVs for k^0 values in the range 0.1–10 cm s^{-1}, using the diffusion coefficient $D_{FcTMA^+} = 7.5 \times 10^{-6}$ cm^2 s^{-1}.[37] Figure 6(b) shows a zoom-in of the region of the LSV in Figure 6(a), where variations in k^0 are most apparent.
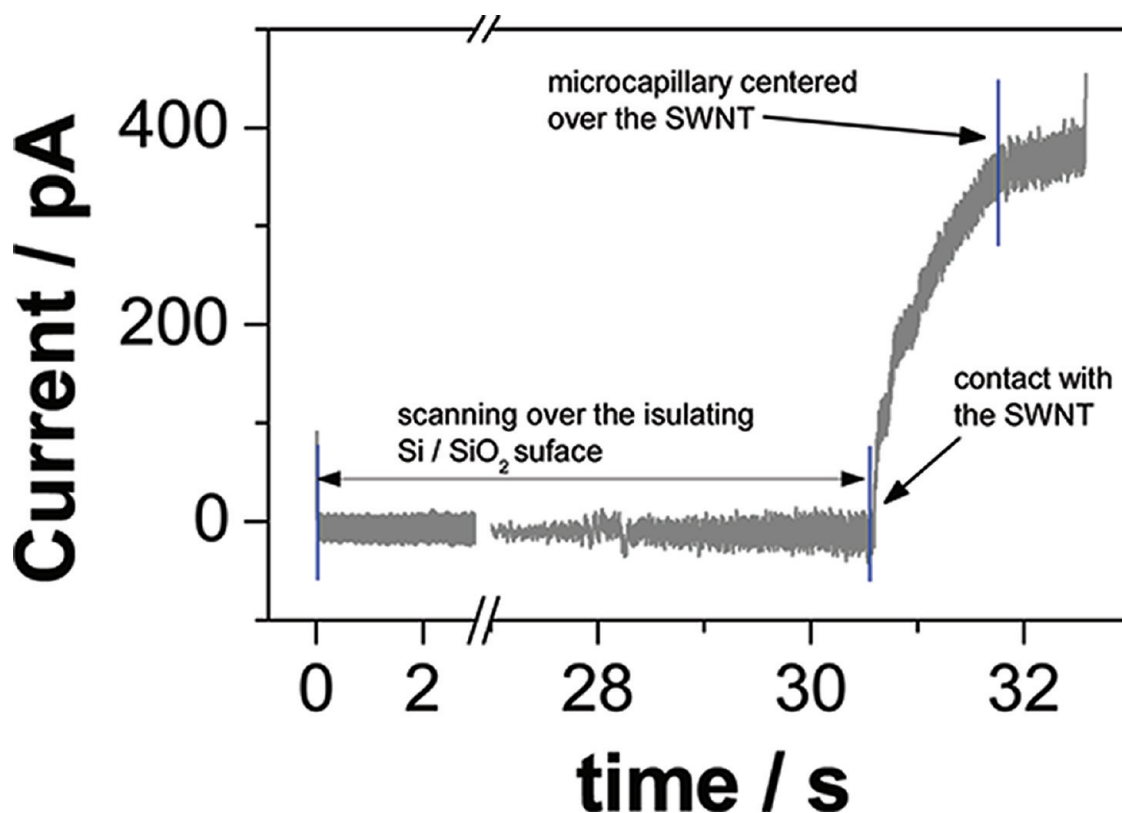
Figure 7. Current−time characteristics for the oxidation of 1 mM FcTMA$^+$ in 0.2 M NaClO$_4$ ($2R_c = 40$ μm and $2R_m = 48$ μm) with the SWNT electrode held at +0.25 V *versus* a Ag/AgCl wire counter/reference electrode. The current−time behavior was recorded once the solution from the capillary had made contact with the insulating SiO$_2$ substrate. As the capillary was manually moved over the substrate, solution contacted the SWNT, giving rise to an electrochemical current. The position of the capillary was maintained fixed once a steady-maximum current had been attained, indicating the SWNT was fully in contact with the solution. Note that this experiment was conducted with the Faraday cage open, which resulted in more significant noise on the trace.

Within the measured error of $E^{0'}$ (SI-2), for eight different experimental LSVs the ET process is essentially reversible. The simulated CVs for FcTMA$^+$ oxidation compared to experiment at different scan rates are found in SI-3. The very close agreement between experiment and simulation confirms the validity of the model, particularly the assumption about the NW geometry.

LSVs for the oxidation of Fe(CN)$_6^{4-}$, at a scan rate of 50 mV s^{-1}, were simulated for k^0 values of 0.01−1 cm s^{-1} (Figure 6(c)) using $D_{\mathrm{Fe(CN)_6^{4-}}} = 6.7 \times 10^{-6}$ cm^2 s^{-1},[38] $R_c = 22.5$ μm, and $R_m = 28$ μm and an exposed NW length of 56 μm. From Figure 6(c), ET kinetics can be clearly resolved, giving $k^0 = 0.08$ cm s^{-1} in this case and yielding $k^0 = 0.10 \pm 0.03$ cm s^{-1} for the range of experimental LSVs recorded (SI-3) using Au NW electrodes. Simulated LSVs for Fe(CN)$_6^{4-}$ oxidation at different scan rates are shown in SI-3. The observed k^0 values agree well with the values recorded using other experimental approaches[30,31] and serve to validate the new nanoscale electrochemical device described herein.

Voltammetry at Individual SWNTs. Higher k^0 values can be discerned by moving to smaller diameter NWs. In these studies the smallest continuous Au NW produced using electrodeposition was ca. 35 nm. However,

ultimately, we cannot produce a NW any smaller than the support SWNT itself, and hence kinetic measurements were carried out on bare SWNTs using the redox couple FcTMA$^{+/2+}$. Such studies are valuable for investigating the intrinsic ET activities of SWNT sidewalls.[39] Moreover, FcTMA$^+$ is oxidized in the potential range where semiconducting SWNTs are in the charge accumulation state and thus should behave in a very similar fashion to metallic SWNTs.[40] Hence it was not essential for us to isolate and identify SWNTs of a particular electronic property.

As the SWNTs could not be visualized under the optical microscope, a quick and easy procedure was developed to enable positioning of the microcapillary over SWNTs. This involved forming a meniscus contact with the SiO$_2$ substrate in the proximity of the evaporated Au contact (typically 20−100 μm away from the contact) and applying a small driving potential, +0.25 V (ca. $E_{1/3}$ for the redox couple of interest), to the working electrode and monitoring the current−time response (Figure 7). The microcapillary was then moved laterally in the x direction, parallel to the gold contact over the sample bearing the SWNTs. In the region of the insulating SiO$_2$ there was no electrochemical current observed, but when the traveling microcapillary
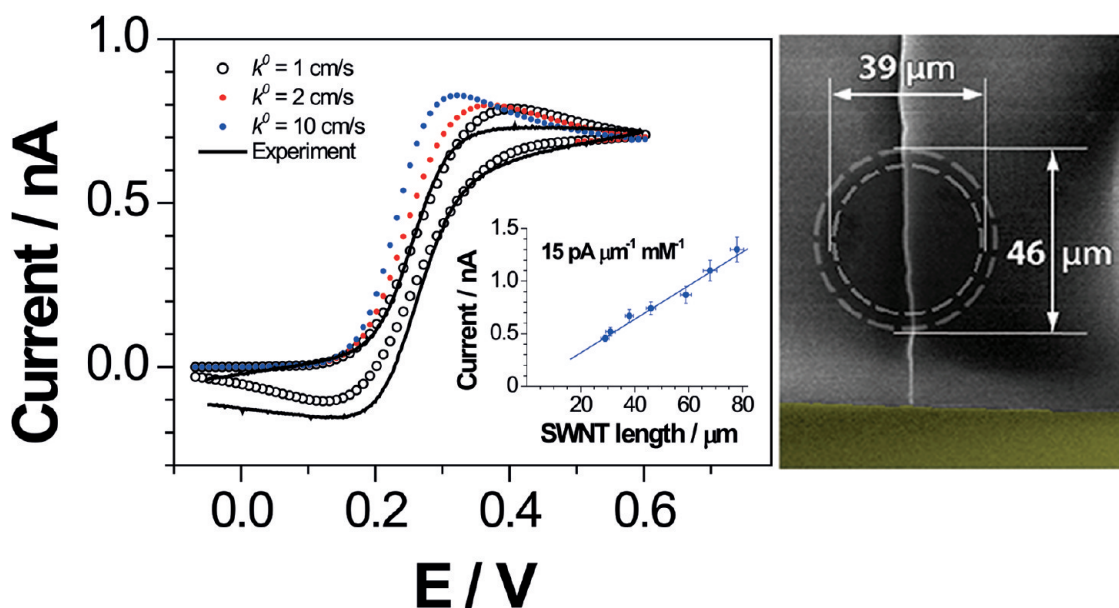
Figure 8. Representative experimental CV for the oxidation of 1 mM FcTMA$^{+/2+}$ in 0.2 M NaClO$_4$ at an individual, <3 nm height, SWNT electrode using a microcapillary with $2R_c = 39$ μm and $2R_m = 46$ μm (determined using FE-SEM) and simulated theoretical fits for FcTMA$^+$ oxidation for different k^0 indicated ($\alpha = 0.5$). The inset shows the experimental dependence of the steady-state current values (at +0.5 V) *vs* contacted SWNT length; error bars represent variation in the experimental values.

meniscus contacted the SWNT, the current increased as an electrochemical cell circuit was completed. The microcapillary tip was then adjusted to the position where the current was observed to be steady and at a maximum value, indicating the SWNT was fully in contact with solution from the end of the capillary and the microcapillary was centered over the SWNT. CVs were recorded in this position. It is evident from Figure 7 that the process of locating a SWNT and positioning the microcapillary can be accomplished in <1 min.

Figure 8 shows a typical CV for the oxidation of 1 mM FcTMA$^+$ in 0.2 M NaClO$_4$ recorded at 100 mV s^{-1} using a microcapillary of $R_c = 19.5$ μm and $R_m = 23$ μm over an individual SWNT with an exposed length of 46 μm. Also shown is a set of simulated CVs with k^0 values in the range 1–10 cm s^{-1} for a 2 nm height SWNT electrode with the above-defined parameters and $h = 15$ μm. The simulated CVs indicate that there should be a slight diffusional peak in the current–voltage response; however for all experiments quasi-steady-state plateau currents ($E > 0.35$ V, high driving potential) were observed. For the case shown in Figure 8 the experimental and simulated curves (using constrained geometric parameters) eventually match at high overpotentials. This was generally, but not always the case (SI-3). Although several fast ET kinetic processes have been analyzed at disk-shaped NSEs[12] and at SWNT devices,[20] recent work indicates that double-layer effects can be significant for disk electrodes at the nanoscale.[41] We are currently investigating the origin of this small deviation using ultrahigh-resolution electrochemical imaging techniques.[26]

Ignoring such effects and examining the results of the simulations it is evident that $k^0 \leq 10$ cm s^{-1} can be readily resolved with this device geometry. Furthermore, the fit in Figure 8 suggests k^0 on the order of 1 cm s^{-1} (fit at low potentials), and kinetic analysis of other experimental CVs (at low potentials) yielded $k^0 = 2 \pm 1$ cm s^{-1} for different SWNTs and different MCEM parameters (SI-3). These observations agree well with previous work, where lower limits for k^0 of >4.6 cm s^{-1} [42] and $k^0 > 1.0 \pm 0.6$ cm s^{-1} [39] were estimated from scanning electrochemical microscopy measurements. Since the double-layer effects, reported by Chen *et al.*,[41] generally push the voltammetric wave shape to greater overpotentials, the values reported here should be treated as minima.

Finally, we found that the diffusion-limited current observed on an individual SWNT scaled with the length of SWNT interrogated (controlled by the size of the microcapillary employed), as shown in the inset to Figure 8. The extracted experimental slope (blue line) gave a value of 15 pA mM^{-1} per μm of SWNT length. It has been suggested by others in the literature[43] that outer-sphere ET on SWNTs occurs only at "*defects*" or "*ends*" and not at the SWNT sidewall. However, in our arrangement no SWNT ends are presented to the electrolyte solution, and if the electrochemistry were driven by "defects", which for the CVD (chemical vapor deposition)-grown SWNTs used herein are of a typical density in the range 1 per 0.1–4 μm SWNT length,[44] the estimated $k^0_{defects}$ would be ~100–4000 cm s^{-1} (minimum range),[39] which is unfeasibly high. Hence, these data are valuable in determining that the side-wall of the SWNT is active for outer-sphere redox

electrochemistry. On the other hand, as pointed out before,[39] we cannot rule out whether a SWNT sidewall may exhibit some heterogeneity in reaction rate, and this may also contribute to some deviation between the experiment and idealized theory that underpins our simulations.

CONCLUSIONS

We have demonstrated a simple approach to fabricate electrochemical cells with individual metallic NW and isolated SWNT working electrodes, using a microcapillary setup (MCEM). The metal NWs are produced using a pulsed electrodeposition approach, where the number of pulses controls the height of the NW; this approach can be applied to any material that can be electrodeposited (*e.g.*, metals, alloys, semiconductors, and conductive polymers). The fabrication methodology employed herein dictates that the NWs and SWNTs are pristine and thus free from lithographic processing contaminants such as photoresist residue. Continuous NWs of the metals Au (height 34−86 nm), Pt (32−90 nm), and Pd (36−110 nm) were produced in this study. Using the simple MCEM setup electrochemical data were collected and, in combination with finite-element modeling, values for k^0 were extracted from voltammetric measurements for both fast and slow ET processes. The SWNT electrode geometry results in a high mass transport rate, which in principle enables analysis of high k^0 values, ≤ 10 cm s^{-1} (for idealized Butler−Volmer kinetics), but we also note a possible double-layer effect that may operate for ET at NSEs fabricated from individual SWNTs. On the other hand, beyond ET kinetics, this arrangement represents a versatile platform for sensing and electroanalytical applications, yielding easily detected signals.

METHODS

SWNT Synthesis. Horizontal millimeter-long SWNT arrays were grown on 1 cm × 1 cm Si wafers ("chips"), with a 300 nm thick layer of SiO$_2$, *via* CVD at 1000 °C using methane (10 sccm) and hydrogen (5 sccm). As the catalyst, 1/200 diluted aqueous ferritin solutions (Sigma Aldrich) were employed,[24] which were deposited, prior to growth, using a ferritin solution-filled capillary (inner diameter 0.69 cm) in a "fountain-pen" manner by manually drawing a catalyst line across the chip. A gold band (70 nm), with a chromium underlayer (2 nm), was evaporated onto the front face of the wafer (with a shadow mask) to provide electrical connection to the aligned SWNTs.

Electrochemical Experiments. All the electrochemical measurements were performed using a potentiostat (CH Instruments model 760, Austin, TX, USA). For the metal wire electrodeposition experiments a commercial Ag|AgCl (3 M KCl) electrode (Dri-ref from World Precision Instruments) was used.

Microcapillary Experiment. Electrochemical measurements at NWs were facilitated by using the microcapillary electrochemical method,[22,25] which employed a glass microcapillary with an inner diameter in the range *ca*. 25−80 μm (precisely measured with an optical microscope), filled with the electrolyte solution of interest, and containing a counter/reference electrode (herein chloride-coated silver wire). A humid cell environment was maintained during the measurement to ensure that evaporation effects from the meniscus of the MCEM are negligible.[22,25]

Raman Spectroscopy. A Renishaw inVia Raman microscope, coupled to a Leica microscope with 50× lens, was used to provide information on the as-grown SWNTs. Given the spacing of the SWNTs in the arrays (typically 100−300 μm) and the spot size of the Raman laser (~3 μm), the intensity of the Raman signal, when sampling an individual SWNT, was too low to provide any meaningful information. To increase the intensity, the SWNTs were decorated with electrodeposited Ag NPs[27] (single pulse of −0.5 V for 1 s duration in a solution containing 1 mM AgNO$_3$ and 0.1 M KNO$_3$ using the setup described above). An Ar laser was employed at an excitation wavelength of 514.5 nm (2.41 eV) at 10 mW power with an exposure time of 30−50 s. SI-4 shows a typical Raman spectra (sampling one SWNT per spectrum), confirming that the as-grown carbon nanotubes were single-walled. The size range of the SWNTs, as measured by AFM (*vide supra*), signifies that some SWNTs form bundles, and hence electrochemical measurements were only made on those <4 nm in height.

Modeling. Finite-element modeling was performed using the Comsol Multiphysics 4.1 package (Comsol AB, Sweden). More detailed information on simulation parameters can be found in SI-2.

High-Resolution Microscopy. AFM (Bruker Nano Enviroscope AFM with a Nanoscope IV controller) and FE SPIP software (Image Metrology) was employed for image analysis. Field emission scanning electron microscopy images were acquired using a SUPRA 55 variable-pressure system (Zeiss) at 1 kV to visualize the SWNTs and at 10 kV to image metal NWs.

REFERENCES AND NOTES

1. Penner, R. M.; Heben, M. J.; Longin, T. L.; Lewis, N. S. Fabrication and Use of Nanometer-Sized Electrodes in Electrochemistry. *Science* **1990**, *250*, 1118−1121.
2. Shao, Y.; Mirkin, M. V.; Fish, G.; Kokotov, S.; Palanker, D.; Lewis, A. Nanometer-Sized Electrochemical Sensors. *Anal. Chem.* **1997**, *69*, 1627−1634.
3. Conyers, J. L.; White, H. S. Electrochemical Characterization of Electrodes with Submicrometer Dimensions. *Anal. Chem.* **2000**, *72*, 4441−4446.
4. Patil, A. V.; Beker, A. F.; Wiertz, F. G. M.; Heering, H. A.; Coslovich, G.; Vlijm, R.; Oosterkamp, T. H. Fabrication and Characterization of Polymer Insulated Carbon Nanotube Modified Electrochemical Nanoprobes. *Nanoscale* **2010**, *2*, 734−738.
5. Krapf, D.; Quinn, B. M.; Wu, M.-Y.; Zandbergen, H. W.; Dekker, C.; Lemay, S. G. Experimental Observation of Nonlinear Ionic Transport at the Nanometer Scale. *Nano Lett.* **2006**, *6*, 2531−2535.

6. Velmurugan, J.; Sun, P.; Mirkin, M. V. Scanning Electrochemical Microscopy with Gold Nanotips: The Effect of Electrode Material on Electron Transfer Rates. *J. Phys. Chem. C* **2008**, *113*, 459–464.

7. Wehmeyer, K. R.; Deakin, M. R.; Wightman, R. M. Electroanalytical Properties of Band Electrodes of Submicrometer Width. *Anal. Chem.* **1985**, *57*, 1913–1916.

8. Chen, S.; Kucernak, A. Electrocatalysis under Conditions of High Mass Transport Rate: Oxygen Reduction on Single Submicrometer-Sized Pt Particles Supported on Carbon. *J. Phys. Chem. B* **2004**, *108*, 3262–3276.

9. Slevin, C. J.; Gray, N. J.; Macpherson, J. V.; Webb, M. A.; Unwin, P. R. Fabrication and Characterisation of Nanometre-Sized Platinum Electrodes for Voltammetric Analysis and Imaging. *Electrochem. Commun.* **1999**, *1*, 282–288.

10. Etienne, M.; Anderson, E. C.; Evans, S. R.; Schuhmann, W.; Fritsch, I. Feedback-Independent Pt Nanoelectrodes for Shear Force-Based Constant-Distance Mode Scanning Electrochemical Microscopy. *Anal. Chem.* **2006**, *78*, 7317–7324.

11. Zhang, B.; Galusha, J.; Shiozawa, P. G.; Wang, G.; Bergren, A. J.; Jones, R. M.; White, R. J.; Ervin, E. N.; Cauley, C. C.; White, H. S. Bench-Top Method for Fabricating Glass-Sealed Nanodisk Electrodes, Glass Nanopore Electrodes, and Glass Nanopore Membranes of Controlled Size. *Anal. Chem.* **2007**, *79*, 4778–4787.

12. Sun, P.; Mirkin, M. V. Kinetics of Electron-Transfer Reactions at Nanoelectrodes. *Anal. Chem.* **2006**, *78*, 6526–6534.

13. Oldham, K. B. A Hole Can Serve as a Microelectrode. *Anal. Chem.* **1992**, *64*, 646–651.

14. Baranski, A. S. On Possible Systematic Errors in Determinations of Charge Transfer Kinetics at Very Small Electrodes. *J. Electroanal. Chem. Interfacial Electrochem.* **1991**, *307*, 287–292.

15. Krapf, D.; Wu, M.-Y.; Smeets, R. M. M.; Zandbergen, H. W.; Dekker, C.; Lemay, S. G. Fabrication and Characterization of Nanopore-Based Electrodes with Radii Down to 2 Nm. *Nano Lett.* **2005**, *6*, 105–109.

16. Day, T. M.; Unwin, P. R.; Wilson, N. R.; Macpherson, J. V. Electrochemical Templating of Metal Nanoparticles and Nanowires on Single-Walled Carbon Nanotube Networks. *J. Am. Chem. Soc.* **2005**, *127*, 10639–10647.

17. Yarden, T. S.; Joselevich, E. Drawing with Nanotubes: Creating Nanowires with Complex Geometries by Pulsed Electrodeposition on Self-Organized Carbon Nanotube Patterns. *Nano Lett.* **2010**, *10*, 4742–4749.

18. Morris, R. B.; Franta, D. J.; White, H. S. Electrochemistry at Platinum Bane Electrodes of Width Approaching Molecular Dimensions: Breakdown of Transport Equations at Very Small Electrodes. *J. Phys. Chem.* **1987**, *91*, 3559–3564.

19. Nagale, M. P.; Fritsch, I. Individually Addressable, Submicrometer Band Electrode Arrays. 2. Electrochemical Characterization. *Anal. Chem.* **1998**, *70*, 2908–2913.

20. Heller, I.; Kong, J.; Heering, H. A.; Williams, K. A.; Lemay, S. G.; Dekker, C. Individual Single-Walled Carbon Nanotubes as Nanoelectrodes for Electrochemistry. *Nano Lett.* **2005**, *5*, 137–142.

21. Amatore, C.; Savéant, J. M.; Tessier, D. Charge Transfer at Partially Blocked Surfaces: A Model for the Case of Microscopic Active and Inactive Sites. *J. Electroanal. Chem. Interfacial Electrochem.* **1983**, *147*, 39–51.

22. Day, T. M.; Unwin, P. R.; Macpherson, J. V. Factors Controlling the Electrodeposition of Metal Nanoparticles on Pristine Single Walled Carbon Nanotubes. *Nano Lett.* **2007**, *7*, 51–57.

23. Dumitrescu, I.; Edgeworth, J. P.; Unwin, P. R.; Macpherson, J. V. Ultrathin Carbon Nanotube Mat Electrodes for Enhanced Amperometric Detection. *Adv. Mater.* **2009**, *21*, 3105–3109.

24. Edgeworth, J. P.; Wilson, N. R.; Macpherson, J. V. Controlled Growth and Characterization of Two-Dimensional Single-Walled Carbon-Nanotube Networks for Electrical Applications. *Small* **2007**, *3*, 860–870.

25. Dudin, P. V.; Unwin, P. R.; Macpherson, J. V. Electrochemical Nucleation and Growth of Gold Nanoparticles on Single-Walled Carbon Nanotubes: New Mechanistic Insights. *J. Phys. Chem. C* **2010**, *114*, 13241–13248.

26. Lai, S. C. S.; Dudin, P. V.; Macpherson, J. V.; Unwin, P. R. Visualizing Zeptomole (Electro)Catalysis at Single Nanoparticles within an Ensemble. *J. Am. Chem. Soc.* **2011**, *133*, 10744–10747.

27. Qian, P.; Wu, Z.; Diao, P.; Zhang, G.; Zhang, J.; Liu, Z. Electrochemical Identification of Metallic and Semiconducting Single-Walled Carbon Nanotubes. *J. Phys. Chem. C* **2008**, *112*, 13346–13348.

28. Walter, E. C.; Murray, B. J.; Favier, F.; Kaltenpoth, G.; Grunze, M.; Penner, R. M. Noble and Coinage Metal Nanowires by Electrochemical Step Edge Decoration. *J. Phys. Chem. B* **2002**, *106*, 11407–11411.

29. Dudin, P. V.; Unwin, P. R.; Macpherson, J. V. Electro-Oxidation of Hydrazine at Gold Nanoparticle Functionalised Single Walled Carbon Nanotube Network Ultramicroelectrodes. *Phys. Chem. Chem. Phys.* **2011**, *13*, 17146–17152.

30. Beriet, C.; Pletcher, D.; Microelectrode, A Study of the Mechanism and Kinetics of the Ferro/Ferricyanide Couple in Aqueous Media: The Influence of the Electrolyte and Its Concentration. *J. Electroanal. Chem.* **1993**, *361*, 93–101.

31. Kawiak, J.; Kulesza, P. J.; Galus, Z. A Search for Conditions Permitting Model Behavior of the $Fe(CN)_6^{3-}/Fe(CN)_6^{4-}$. *J. Electroanal. Chem. Interfacial Electrochem.* **1987**, *226*, 305–314.

32. Heras, A.; Colina, A.; Ruiz, V.; López-Palacios, J. UV-Visible Spectroelectrochemical Detection of Side-Reactions in the Hexacyanoferrate(III)/(II) Electrode Process. *Electroanalysis* **2003**, *15*, 702–708.

33. Campbell, S. A.; Peter, L. M. The Effect of $[K^+]$ on the Heterogeneous Rate Constant for the $[Fe(CN)_6]^{3-}/[Fe(CN)_6]^{4-}$ Redox Couple Investigated by A.C. Impedance Spectroscopy. *J. Electroanal. Chem.* **1994**, *364*, 257–260.

34. Bard, A. J. Inner-Sphere Heterogeneous Electrode Reactions. Electrocatalysis and Photocatalysis: The Challenge. *J. Am. Chem. Soc.* **2010**, *132*, 7559–7567.

35. Alvarez-Ruiz, B.; Gomez, R.; Orts, J. M.; Feliu, J. M. Role of the Metal and Surface Structure in the Electro-Oxidation of Hydrazine in Acidic Media. *J. Electrochem. Soc.* **2002**, *149*, D35–D45.

36. Eisner, U.; Zemer, Y. Anodic Oxidation of Hydrazine and Its Derivatives: Part Iv. The Oxidation of Methylhydrazine (Mh) on Gold Electrodes in Acid Solution. *J. Electroanal. Chem.* **1972**, *38*, 381–388.

37. Yuan, L.; Macartney, D. H. Kinetics of the Electron Self-Exchange and Electron-Transfer Reactions of the (Trimethylammonio)Methylferrocene Host−Guest Complex with Cucurbit[7]Uril in Aqueous Solution. *J. Phys. Chem. B* **2007**, *111*, 6949–6954.

38. Macpherson, J. V.; Unwin, P. R. Radial Flow Microring Electrode: Development and Characterization. *Anal. Chem.* **1998**, *70*, 2914–2921.

39. Dumitrescu, I.; Dudin, P. V.; Edgeworth, J. P.; Macpherson, J. V.; Unwin, P. R. Electron Transfer Kinetics at Single-Walled Carbon Nanotube Electrodes Using Scanning Electrochemical Microscopy. *J. Phys. Chem. C* **2010**, *114*, 2633–2639.

40. Day, T. M.; Wilson, N. R.; Macpherson, J. V. Electrochemical and Conductivity Measurements of Single-Wall Carbon Nanotube Network Electrodes. *J. Am. Chem. Soc.* **2004**, *126*, 16724–16725.

41. Liu, Y.; He, R.; Zhang, Q.; Chen, S. Theory of Electrochemistry for Nanometer-Sized Disk Electrodes. *J. Phys. Chem. C* **2010**, *114*, 10812–10822.

42. Kim, J.; Xiong, H.; Hofmann, M.; Kong, J.; Amemiya, S. Scanning Electrochemical Microscopy of Individual Single-Walled Carbon Nanotubes. *Anal. Chem.* **2010**, *82*, 1605–1607.

43. Dumitrescu, I.; Unwin, P. R.; Macpherson, J. V. Electrochemistry at Carbon Nanotubes: Perspective and Issues. *Chem. Commun.* **2009**, 6886–6901.

44. Fan, Y.; Goldsmith, B. R.; Collins, P. G. Identifying and Counting Point Defects in Carbon Nanotubes. *Nat. Mater.* **2005**, *4*, 906–911.